

## Joint Scalar and Velocity-Scalar PDF Modelling of a Bluff-Body Stabilised Flame

B. Merci<sup>\*,1,2</sup>, B. Naud<sup>3</sup>, D. Roekaerts<sup>4</sup> and U. Maas<sup>5</sup>

<sup>1</sup> Postdoctoral Fellow of the Fund of Scientific Research – Flanders (Belgium) (FWO-Vlaanderen)

<sup>2</sup> Ghent University – UGent, Dept. of Flow, Heat and Combustion Mechanics, Ghent, Belgium

<sup>3</sup> Modeling and Numerical Simulation Group, Energy Dept., Ciemat, Madrid, Spain

<sup>4</sup> Dept. of Multi-Scale Physics, Delft University of Technology, Delft, The Netherlands

<sup>5</sup> Institute for Technical Thermodynamics, Karlsruhe University (TH), Germany

### Abstract

A comparative study is presented of joint velocity-scalar and joint scalar PDF results for ‘Sydney Flame HM1’. This jet type turbulent flame is stabilized behind a bluff body. Chemistry is modeled by means of the Intrinsic Low-Dimensional Manifold (ILDM) technique, based on mixture fraction and two progress variables ( $CO_2$  and  $H_2O$  mass fractions). In the comparison, the turbulence model (Reynolds stress type) and the micro-mixing model (modified Curl’s coalescence/dispersion) are kept the same. The mean velocity and turbulent stresses are very similar in both calculations. On the other hand, significant differences in the radial profiles of mean scalars and of mixture fraction variance are observed. This is explained from the fact that the two PDF approaches considered, imply different closures for the velocity-scalar correlation. In other words, the scalar flux modeling is different. The velocity-scalar PDF implies a differential scalar flux model, while scalar PDF results correspond to gradient diffusion. It is found that the velocity-scalar PDF results are in general in better agreement with the experimental data. Results in composition space, visualized as scatter plots, confirm the higher quality of the velocity-scalar PDF.

### Introduction

In turbulent non-premixed flames, the non-linear interaction between turbulent fluctuations and finite-rate chemistry often plays an important role. When the interactions are sufficiently strong, this may lead to local extinction or incomplete combustion. Turbulence-chemistry interaction is therefore a central issue in non-premixed turbulent flame modeling in numerical simulations. At the level of the transported probability density function (PDF) technique, be it joint scalar or joint velocity-scalar, an exact treatment of the chemical reaction source term, given a certain chemistry model, is achieved [1].

We apply transported PDF methods based on stochastic Lagrangian modeling. As described in [1], a transport equation for the mass density function (MDF) is modeled and solved using a particle stochastic method. Three major modeling ingredients are necessary: a turbulence model, a chemistry model and a micro-mixing model. Several recent comparative studies focused on the influence of those different sub-models on numerical simulation results of turbulent non-premixed flames. In [2] for instance, three widely used micro-mixing models are compared, considering stochastic simulations of partially stirred reactors (PaSR). In the context of transported scalar PDF modeling, the same micro-mixing models are compared in [3] for the piloted jet diffusion flame Delft flame III, and in [4] for the bluff-body stabilized flames ‘Sydney HM1-3’. In [5], seven combustion mechanisms for methane/air are compared for joint velocity-scalar-turbulence frequency PDF calculations of the non-premixed piloted jet flames ‘Sandia D-F’. In [6], the

influence of three  $C_1$  chemistry models on two micro-mixing models is studied for Delft flame III and the bluff-body flames HM1-3.

In addition to the three sub-models mentioned, the PDF description itself has direct consequences on the modeling of the scalar flux (and higher order velocity-scalar correlation). When considering the joint scalar MDF  $F_\phi$ , the use of a gradient diffusion assumption to close the conditional fluctuating velocity term in the MDF transport equation, results in a simple algebraic model for the scalar flux. When velocity is included in the PDF description, the transport equation for the joint velocity-scalar MDF  $F_{U\phi}$ , is modeled and solved using a particle method. In this case, a modeled transport equation for the scalar flux (and for higher order velocity-scalar correlation) is implied.

In the following, numerical simulation results are compared of scalar PDF and velocity-scalar PDF calculations. All calculations are performed with the same hybrid Finite-Volume / particle methods, as implemented in the same in-house computer program ‘PDFD’ [7], with the same turbulence, chemistry and micro-mixing models. The flame considered is the Sydney bluff-body stabilized flame HM1 [8, 9, 10], a target flame of the International Workshop on Measurement and Computation of Turbulent Non-premixed Flames [11]. On [11], detailed descriptions are also found for the other flames, mentioned in this introduction (Delft Flame III and Sandia Flames D-F).

\* Corresponding author: [Bart.Merci@UGent.be](mailto:Bart.Merci@UGent.be)

## Specific objectives

As mentioned in the introduction, the major objective of the present study is to evaluate differences in numerical simulation results of a turbulent non-premixed bluff-body stabilized flame, caused by different PDF formulations (joint scalar vs. joint velocity-scalar). All other sub-models and numerical aspects (including the computational mesh), are kept identical in order to focus the study as much as possible.

## Results and Discussion

We first describe the approach and then discuss the results. Not everything is described in full detail. The reader is referred to reference [27].

### PDF Approaches

The statistical description of the flow is in terms of the joint one-point PDF  $f_\phi$ :  $f_\phi(\Psi; \mathbf{x}, t) d\Psi$  is the probability that  $\Phi$  is in the interval  $[\Psi, \Psi + d\Psi]$  at point  $(\mathbf{x}, t)$ . Considering the joint scalar PDF,  $\Phi$  is the composition vector  $\phi$ . In the framework of the joint velocity-scalar PDF approach,  $\Phi = (\mathbf{U}, \phi)$ , with  $\mathbf{U}$  the velocity vector.

The joint PDF is defined as [1, 12]:

$$f_\phi(\Psi; \mathbf{x}, t) = \langle \delta[\Phi(\mathbf{x}, t) - \Psi] \rangle \quad (1)$$

where  $\delta[\ ]$  is the Dirac delta function and where the brackets  $\langle \ \rangle$  refer to expected values [12].

Using the conditional expected value [1], mean values (or expected values) are defined as:

$$\langle Q(\mathbf{x}, t) \rangle = \int_{[\Psi]} \langle Q(\mathbf{x}, t) | \Psi \rangle f_\phi(\Psi; \mathbf{x}, t) d\Psi \quad (2)$$

Fluctuations are defined as:  $q'(\mathbf{x}, t) = Q(\mathbf{x}, t) - \langle Q(\mathbf{x}, t) \rangle$ .

For variable density flows, it is useful to consider the mass density function (MDF)  $F_\phi(\Psi) = \rho(\Psi) f_\phi(\Psi)$ . Density weighted averages (Favre averages) can then be considered. Fluctuations with respect to the Favre average are defined as:  $q''(\mathbf{x}, t) = Q(\mathbf{x}, t) - \tilde{Q}(\mathbf{x}, t)$ .

When the joint scalar MDF  $F_\phi$  is considered, the following transport equation is modelled and solved [1]:

$$\begin{aligned} \frac{\partial F_\phi}{\partial t} + \frac{\partial \tilde{U}_j F_\phi}{\partial x_j} + \frac{\partial}{\partial \psi_\alpha} [S_\alpha(\psi) F_\phi] \\ = - \underbrace{\frac{\partial}{\partial x_i} [\langle u_i'' | \psi \rangle F_\phi]}_{\text{gradient diffusion}} - \frac{\partial}{\partial \psi_\alpha} \left[ \underbrace{\frac{1}{\rho(\psi)} \left\langle - \frac{\partial J_j^\alpha}{\partial x_j} \right| \psi \right]}_{\text{mixing model: } \theta_\alpha} F_\phi \end{aligned} \quad (3)$$

where  $S_\alpha$  is the reaction source term for scalar  $\phi_\alpha$  and  $\mathbf{J}^\alpha$  its molecular flux.

When velocity is included in the PDF description, the transport equation for the joint velocity-scalar MDF  $F_{U\phi}$  can be written (neglecting the mean viscous stress tensor gradient  $\partial \langle \tau_{ij} \rangle / \partial x_j$ ):

$$\begin{aligned} \frac{\partial F_{U\phi}}{\partial t} + V_j \frac{\partial F_{U\phi}}{\partial x_j} \\ + \left( - \frac{1}{\rho(\psi)} \frac{\partial \langle p \rangle}{\partial x_i} + g_i \right) \frac{\partial F_{U\phi}}{\partial V_i} + \frac{\partial}{\partial \psi_\alpha} [S_\alpha(\psi) F_{U\phi}] \\ = - \frac{\partial}{\partial V_i} \left[ \underbrace{\frac{1}{\rho(\psi)} \left\langle - \frac{\partial p'}{\partial x_i} + \frac{\partial \tau'_{ij}}{\partial x_j} \right| \mathbf{V}, \psi \right]}_{\text{Langevin model: } a_i} F_\phi \\ - \frac{\partial}{\partial \psi_\alpha} \left[ \underbrace{\frac{1}{\rho(\psi)} \left\langle - \frac{\partial J_j^\alpha}{\partial x_j} \right| \mathbf{V}, \psi \right]}_{\text{mixing model: } \theta_\alpha} F_\phi \end{aligned} \quad (4)$$

The above equations are solved using the consistent hybrid Finite-Volume / particle method presented in [2]. Mean velocity  $\tilde{\mathbf{U}}$ , mean pressure gradient  $\partial \langle p \rangle / \partial x_i$ , Reynolds stresses  $\langle \rho u_i'' u_j'' \rangle$  and turbulent dissipation  $\varepsilon$  are solved using a standard Finite-Volume (FV) method based on a pressure-correction algorithm. A particle method is applied for the solution of the MDF transport equation, as described in [27]. A set of uniformly distributed computational particles evolves according to stochastic differential equations. Each particle has a set of properties  $\{w^*, m^*, \mathbf{X}^*, \phi^*\}$  (scalar MDF), or  $\{w^*, m^*, \mathbf{X}^*, \mathbf{u}^*, \phi^*\}$  (velocity-scalar MDF), where  $w^*$  is a numerical weight,  $m^*$  is the particle mass,  $\mathbf{X}^*$  its position,  $\mathbf{u}^*$  its fluctuating velocity and  $\phi^*$  the particle's composition. The superscript \* denotes that the quantity is a stochastic particle property. The method of fractional steps [1] is used to integrate the systems of equations. In order to ensure second-order accuracy, the 'midpoint rule' is used [13, 14]. A local time-stepping algorithm developed in the framework of statistically stationary problems [15] is applied.

Turbulent dissipation is not included in the PDF representation. The transport equation solved for  $\varepsilon$  in the FV method provides extra information for modeling the unclosed terms  $a_i$  and  $\theta_\alpha$ . The other FV equations are consistent with the modeled MDF transport equation [7].

The mean density in the FV method is directly obtained from the iteration averaged mean density in the particle method (the iteration averaging procedure presented in [7] is used).

An outer iteration consists of a number of FV iterations and particle time steps. We use a fixed number of particle time steps (typically 5), while the FV method is iterated until the residuals of all equations start decreasing and the global mean pressure correction is below a specified threshold (with a maximum of 1000 FV iterations per outer iteration).

## Modeling

In the context of RANS, turbulence is modeled using a second-moment closure. As argued in [16], the LRR isotropization of production model (LRR-IPM) of [17] is applied, with modified constant value  $C_{\varepsilon I} = 1.6$ ,

instead of the standard value  $C_{\varepsilon l} = 1.44$ . Consistently, the Lagrangian isotropization of production model (LIPM) is used in the velocity-scalar PDF approach to describe velocity evolution  $a_i$  [18, 19].

For the chemical combustion reactions, the intrinsic low-dimensional manifold (ILDM) method is applied in order to reduce the number of degrees of freedom compared to detailed reaction mechanisms [20]. Fuel (50%  $CH_4$  and 50%  $H_2$  by volume) and air are assumed to react in a two-stream, adiabatic system, with the assumption of equal diffusivities and unity Lewis number (both streams at atmospheric pressure and at a temperature of 298K). The resulting reduced chemistry is parameterized by three control variables: mixture fraction ( $\xi$ ), and  $CO_2$  and  $H_2O$  mass fractions ( $Y_{CO_2}$  and  $Y_{H_2O}$ ). The mixture fraction  $\xi$  is defined on the basis of Bilger's formula [21]:

$$\xi = \frac{\frac{2(Z_C - Z_{C,o})}{W_C} + \frac{(Z_H - Z_{H,o})}{2W_H} - \frac{Z_O - Z_{O,o}}{W_O}}{\frac{2(Z_{C,f} - Z_{C,o})}{W_C} + \frac{(Z_{H,f} - Z_{H,o})}{2W_H} - \frac{Z_{O,f} - Z_{O,o}}{W_O}} \quad (5)$$

where  $Z_\beta$  is the total mass fraction of element  $\beta$  and  $W_\beta$  is its atomic mass. The subscripts "f" and "o" refer to the fuel and oxidant streams.

In equations (3) and (4),  $\boldsymbol{\varphi} = (\xi, Y_{CO_2}, Y_{H_2O})$ , and the chemical source terms  $S_{CO_2}(\boldsymbol{\varphi})$  and  $S_{H_2O}(\boldsymbol{\varphi})$  are obtained from the ILDM reduced scheme.

As mixing model  $\theta_\alpha$ , the modified Curl's coalescence dispersion (CD) model is used. This micro-mixing model prescribes the evolution of particle composition as a series of pair-wise mixing events. The participating mixing particles are chosen at random from the set of particles present in a finite volume cell and their compositions change in the direction of the partner. The degree of mixing in a pair is determined by a random variable uniformly distributed between 0 (no mixing) and 1 (complete mixing) [22, 23].

The chosen models imply modeled transport equations for mean scalars and scalar variance:

$$\frac{\partial \langle \rho \tilde{\varphi}_\alpha \rangle}{\partial t} + \frac{\partial \langle \rho \tilde{\varphi}_\alpha \tilde{U}_j \rangle}{\partial x_j} = - \frac{\partial \langle \rho u_j'' \varphi_\alpha'' \rangle}{\partial x_j} + \langle \rho \tilde{S}_\alpha \rangle \quad (6)$$

$$\begin{aligned} & \frac{\partial \langle \rho \varphi_\alpha''^2 \rangle}{\partial t} + \frac{\partial \langle \rho \varphi_\alpha''^2 \tilde{U}_j \rangle}{\partial x_j} + 2 \langle \rho u_j'' \varphi_\alpha'' \rangle \frac{\partial \tilde{\varphi}_\alpha}{\partial x_j} \\ & = - \frac{\partial \langle \rho u_j'' \varphi_\alpha''^2 \rangle}{\partial x_j} - 2 \langle \rho \varphi_\alpha'' S_\alpha \rangle - 2 \langle \rho \varphi_\alpha'' \theta_\alpha \rangle \end{aligned} \quad (7)$$

with no implicit summation on  $\alpha$ . In the latter equation, the modeling of the last term (scalar dissipation and molecular diffusion) results from the mixing model  $\theta_\alpha$  and is the same in both PDF approaches.

There is a difference, though, in the modeling of the scalar flux, which is implied by the transported MDF method (joint scalar or joint velocity-scalar). When the modeled joint scalar MDF is solved, the gradient diffusion assumption (random walk model in the particle method) implies the following algebraic models for velocity-scalar correlation:

$$\langle \rho u_j'' \varphi_\alpha'' \rangle = -\Gamma_T \frac{\partial \tilde{\varphi}_\alpha}{\partial x_j}; \quad \langle \rho u_j'' \varphi_\alpha''^2 \rangle = -\Gamma_T \frac{\partial \tilde{\varphi}_\alpha''^2}{\partial x_j} \quad (8)$$

When the joint velocity-scalar MDF is considered, a differential scalar flux model is in fact implied, depending on the Langevin model  $a_i$  and the mixing model  $\theta_\alpha$ . For instance, the modeled scalar flux transport equation takes the form:

$$\begin{aligned} & \frac{\partial \langle \rho u_i'' \varphi_\alpha'' \rangle}{\partial t} + \frac{\partial \langle \rho u_i'' \varphi_\alpha'' \tilde{U}_j \rangle}{\partial x_j} \\ & + \langle \rho u_j'' \varphi_\alpha'' \rangle \frac{\partial \tilde{U}_i}{\partial x_j} + \langle \rho u_i'' u_j'' \rangle \frac{\partial \tilde{\varphi}_\alpha}{\partial x_j} \\ & = - \frac{\partial \langle \rho u_i'' u_j'' \varphi_\alpha'' \rangle}{\partial x_j} + \langle \rho u_i'' S_\alpha \rangle + \langle \rho a_i \varphi_\alpha'' \rangle + \langle \rho u_i'' \theta_\alpha \rangle \end{aligned} \quad (9)$$

This affects the results, as is discussed below.

## Test Case

Gaseous fuel (50%  $H_2$  and 50%  $CH_4$  by volume), is injected in the centre of the bluff-body burner (central diameter  $D_j = 3.6\text{mm}$ ). The bluff body, with outer diameter  $D_b = 50\text{mm}$ , is surrounded by an unconfined co-flowing air stream. Fuel and air are mixed in the recirculation zone behind the bluff body where chemical reaction can occur. The hot products stabilize the flame. In the experimental studies [8] and [9], the jet and co-flow bulk velocities were 118m/s, resp. 40m/s (flame HM1). More recently, two sets of velocity measurements were provided [10] for reduced jet and co-flow bulk velocities of 108m/s, resp. 35m/s (flame HM1e). The reader is referred to [11] for a more complete description.

The numerical settings are similar to [7]. A  $6D_b$  long and  $3D_b$  wide two-dimensional computational domain is used. Free-slip boundary conditions are prescribed on the bluff-body surface and on the lateral boundary. A convective outlet boundary condition [24] is used in order to avoid reflecting waves. Inlet boundary conditions are specified at cell centers, as in [25]. The simulations are performed on a  $160 \times 128$  Cartesian grid, stretched both in axial and radial directions.

An average number of 100 particles per cell is used. Iteration averages are made over 500 iterations. The coupling between FV and particle methods is done as described above. As in [7], converged results, obtained using an assumed-shape PDF method, are used as initial conditions. About 1000 outer iterations (5000 particle time steps) are sufficient to reach a stationary solution. Results obtained after 15000 particle time steps are now discussed.

## Results in Physical Space

The mean flow field, including Reynolds stresses, is discussed in [27]. An important observation is that differences between scalar PDF and velocity-scalar PDF

results, due to some differences in mean density, are negligible for the test case under study.

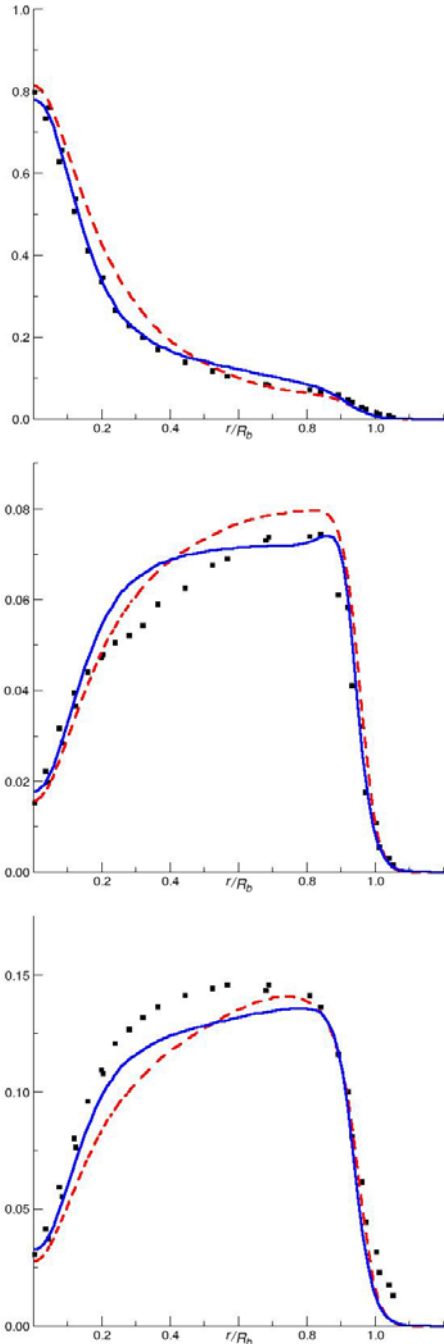


Fig. 1. Profiles of mean mixture fraction (top),  $Y_{CO_2}$  (middle) and  $Y_{H_2O}$  (bottom) at  $x = 0.6D_b$  (inside recirculation region). [Dashed line: joint scalar PDF; solid line: joint velocity-scalar PDF.]

Fig. 1 shows mean radial profiles for the three scalars  $\zeta$ ,  $Y_{CO_2}$  and  $Y_{H_2O}$ . Significant differences between the joint scalar and joint velocity-scalar PDF results are observed. It is not clear what results are the best for  $Y_{CO_2}$  and  $Y_{H_2O}$ . For mean mixture fraction, best results are obtained with the joint velocity-scalar PDF approach. The observed differences can be explained from the mean transport equation, as described above. As suggested by mean velocity and Reynolds stress results,

the influence of mean density can be neglected. Hence, for mixture fraction (no reaction source term), the difference is due to the different modeling of the scalar flux  $\langle \rho u_j'' \xi'' \rangle$ . The relative differences observed for  $Y_{CO_2}$  and  $Y_{H_2O}$  are similar to those observed for  $\zeta$  for similar mean gradients (be it with opposite sign). This suggests that scalar flux modeling is also the major source of difference for the reacting scalars.

In Fig. 2, differences are also shown in the radial profiles of mixture fraction variance. In general, velocity-scalar PDF results are in better agreement with the experimental data. The observed differences are related to the modeling of velocity-scalar correlation: the scalar flux  $\langle \rho u_j'' \xi'' \rangle$  appearing in the production term and the triple correlation  $\langle \rho u_j'' \xi'' \xi'' \rangle$  appearing in the turbulent diffusion term.

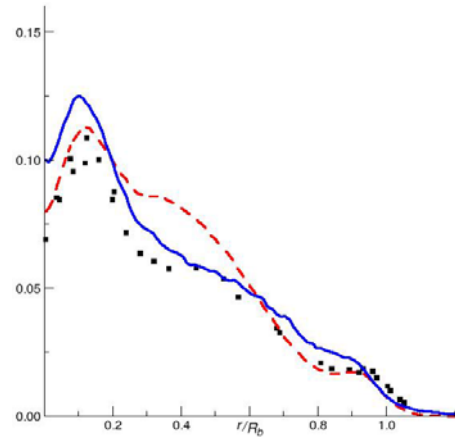


Fig. 2. Mixture fraction variance at  $x = 0.6D_b$ . [Dashed line: joint scalar PDF; solid line: joint velocity-scalar PDF.]

In [27], profiles are also presented at other locations. In general, the better agreement with the joint velocity-scalar approach is confirmed.

### Scatter Plots

The above observations are to be expected. The higher quality of a differential scalar flux model, as compared to a gradient diffusion assumption, particularly in a flow with a strong recirculation zone, is in line with the expectations. We now focus on the impact of the choice of the PDF method on the predicted joint PDF of  $\zeta$  and  $Y_{CO_2}$ . In [27], a similar study is presented for the joint PDF of  $\zeta$  and  $Y_{H_2O}$ , with similar results.

The scatter plots of  $Y_{CO_2}$ , shown in Fig. 3, reveal the strong impact of the PDF method on the predicted joint PDF at the radial cross section  $x=13\text{mm}$ . For the considered CD mixing model, at the lean side, the scalar PDF shows remarkably more particles at fully burnt conditions than the velocity-scalar PDF. The latter is clearly in better qualitative agreement with the experiment. This trend is still observed in at  $x=30\text{mm}$  (Fig. 4). However, further downstream, at  $x=65\text{mm}$ ,

scalar PDF and velocity-scalar PDF methods lead to similar shapes of the joint PDF (Fig. 5). The joint scalar PDF study of [4] suggests that this could be related to the tendency of the CD mixing model towards uniform conditional fluctuation intensity downstream of the recirculation region. Further studies are required in order to clarify this point.

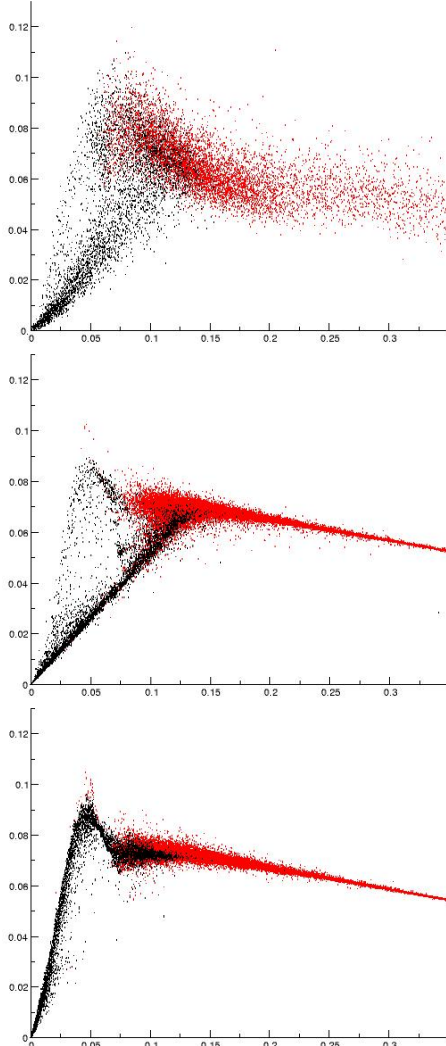


Fig. 3. Scatter plots of  $Y_{CO_2}$  at  $x = 0.13D_b$ . Top: experiments; middle: joint velocity-scalar PDF; bottom: joint scalar PDF.

As a final remark, we note that the level of scatter in the present results, obtained with the CD mixing model, is in better agreement with the experimental data than in the results of [26]. The latter results were obtained with the EMST mixing model. This is in fact the reason for choosing the CD mixing model in the present study. As discussed in [26], there are notable differences between the micro-mixing model behavior in joint scalar PDF results for HM1 and HM2 or HM3 (which are flames with stronger turbulence – chemistry interaction). The possible effect in the joint velocity-scalar PDF approach remains to be investigated.

## Conclusions

A fair comparison has been presented of scalar PDF and velocity-scalar PDF modeling of the non-premixed turbulent bluff-body flame HM1. Whereas differences in the mean flow field are negligible (not shown here), significant differences are observed in results for mean scalars and mixture fraction variance.

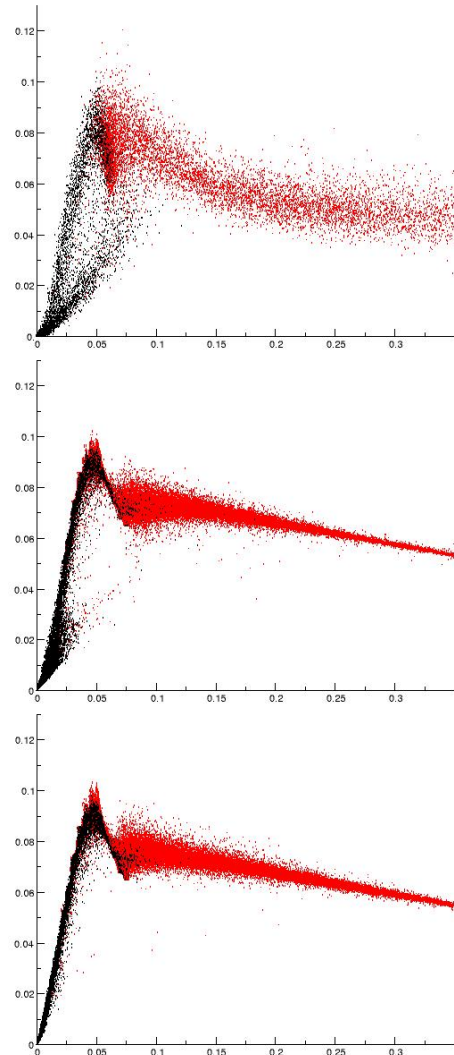


Fig. 4. Scatter plots of  $Y_{CO_2}$  at  $x = 0.3D_b$ . Top: experiments; middle: joint velocity-scalar PDF; bottom: joint scalar PDF.

Not surprisingly, velocity-scalar PDF results (implying a differential scalar flux model) are in general better than scalar PDF results (based on gradient diffusion assumption).

Results in composition space give more direct information on how effects of mixing and reaction combine. With the CD mixing model used in this study, best qualitative agreement of scatter plots, particularly in the near field ( $x=0.13D_b$ ), are obtained with the velocity-scalar PDF.

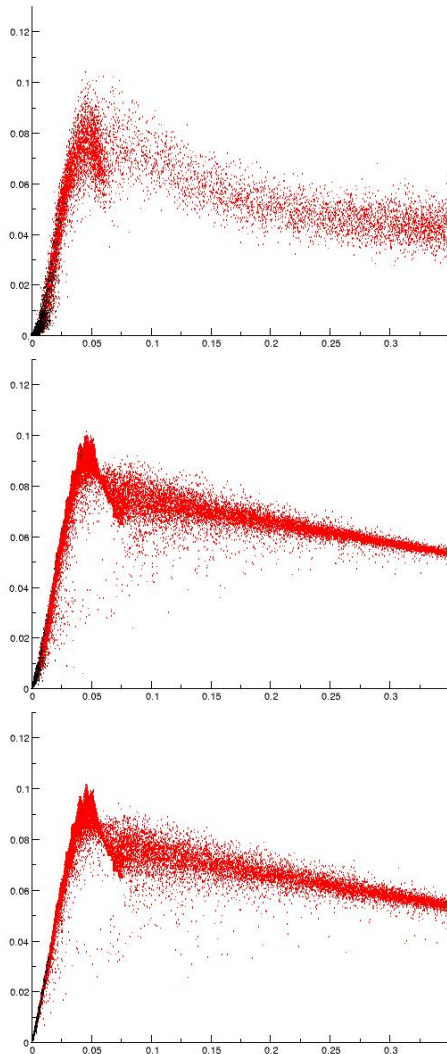


Fig. 5. Scatter plots of  $Y_{CO_2}$  at  $x = 0.65D_b$ . Top: experiments; middle: joint velocity-scalar PDF; bottom: joint scalar PDF.

### Acknowledgements

This collaborative research is supported by the COMLIMANS program, by the Spanish MEC under Project ENE 2005-09190-C04-04/CON and by the Fund of Scientific Research – Flanders (Belgium) (FWO-Vlaanderen) through FWO-project G.0070.03.

### References

1. S.B. Pope. *Prog. En. Combust. Sci.*, 11:119-192, 1985.
2. Z. Ren and S.B. Pope. *Combust. Flame*, 136:208-216, 2004.
3. B. Merci, D. Roekaerts and B. Naud. *Combust. Flame*, 144:476-493, 2006.
4. B. Merci, D. Roekaerts, B. Naud and S.B. Pope. *Combust. Flame* 146:109-130, 2006.
5. R.R. Cao and S.B. Pope. *Combust. Flame*, 143:450-470, 2005.
6. B. Merci, B. Naud and D. Roekaerts. *Combust. Sci. Technol.* 179: 153 -172, 2007.
7. B. Naud, C. Jiménez and D. Roekaerts. *Prog. Comp. Fluid Dyn.*, 6:146-157, 2006.
8. B.B. Dally and A.R. Masri. *Combust. Theory Mod.*, 2:193-219, 1998.
9. B.B. Dally, A.R. Masri, R.S. Barlow, and G.J. Fiechtner. *Combust. Flame*, 114:119-148, 1998.
10. [http://www.aeromech.usyd.edu.au/thermofluids/main\\_frame.htm](http://www.aeromech.usyd.edu.au/thermofluids/main_frame.htm)
11. R.S. Barlow. International Workshop on Measurement and Computation of Turbulent Nonpremixed Flames. <http://www.ca.sandia.gov/TNF>
12. S.B. Pope. *Turbulent Flows*, Cambridge University Press, 2000.
13. M. Muradoglu, S.B. Pope, and D.A. Caughey. *J.Comp. Phys.*, 172:841-878, 2001.
14. P. Jenny, S.B. Pope, M. Muradoglu, and D.A. Caughey. *J. Comp. Phys.*, 166:218-252, 2001.
15. M. Muradoglu and S.B. Pope. *AIAA J.*, 40:1755-1763, 2002.
16. G. Li, B. Naud and D. Roekaerts. *Flow, Turbul. Combust.*, 70:211-240, 2003.
17. B.E. Launder, G.J. Reece and W. Rodi. *J. Fluid Mech.*, 68:537-566, 1975.
18. S.B. Pope. *Phys. Fluids*, 6:973-985, 1994.
19. H.A. Wouters, T.W.J. Peeters and D. Roekaerts. *Phys. Fluids*, 8:1702-1704, 1996.
20. U. Maas and S.B. Pope. *Combust. Flame*, 88:239-264, 1992.
21. R.W. Bilger, S.H. Starner and R.J. Kee. *Combust. Flame*, 80:135-149, 1990.
22. J. Janicka, W. Kolbe and W. Kollmann. *J. Non-Equil. Thermod.*, 4:47-66, 1979.
23. H.A. Wouters, T.W.J. Peeters, and D. Roekaerts. Chapter 2 in *Closure strategies for turbulent and transitional flows* (Edited by B. Launder and N. Sandham), Cambridge University Press, pp. 626-655, 2002.
24. A. Sohankar, C. Norberg, and L. Davidson. *Int. J. Num. Meth. Fluids*, 26:39-56, 1998.
25. M. Muradoglu, K. Liu, and S.B. Pope. *Combust. Flame*, 132:115-137, 2003.
26. K. Liu, S.B. Pope and D.A. Caughey. *Combust. Flame*, 141:89-117, 2005.
27. B. Naud, B. Merci, D. Roekaerts, D. Schmidt and U. Maas, Scalar PDF and velocity-scalar PDF modelling of the bluff-body stabilised flame HM1 using ILDM, *Flow, Turbul. Combust.* (in review).